Jyväskylän yliopiston julkaisuarkisto
Jyväskylä University Digital Archive

UNIVERSITY OF JYVÄSKYLÄ

This is an electronic reprint of the original article.
This reprint *may differ* from the original in pagination and typographic detail.

Author(s): Gu, Yufei; Lensu, Anssi; Perämäki, Siiri; Ojala, Anna; Vähätalo, Anssi

Title: Iron and pH Regulating the Photochemical Mineralization of Dissolved Organic Carbon

Year: 2017

Version:

Please cite the original version:

Gu, Y., Lensu, A., Perämäki, S., Ojala, A., & Vähätalo, A. (2017). Iron and pH Regulating the Photochemical Mineralization of Dissolved Organic Carbon. ACS Omega, 2(5), 1905-1914. https://doi.org/10.1021/acsomega.7b00453

All material supplied via JYX is protected by copyright and other intellectual property rights, and duplication or sale of all or part of any of the repository collections is not permitted, except that material may be duplicated by you for your research use or educational purposes in electronic or print form. You must obtain permission for any other use. Electronic or print copies may not be offered, whether for sale or otherwise to anyone who is not an authorised user.

This is an open access article published under an ACS AuthorChoice License, which permits copying and redistribution of the article or any adaptations for non-commercial purposes.

ACS OMEGA

Article

http://pubs.acs.org/journal/acsodf

Iron and pH Regulating the Photochemical Mineralization of Dissolved Organic Carbon

Yufei Gu,*[,†] Anssi Lensu,[†] Siiri Perämäki,[‡] Anne Ojala,[§,∥] and Anssi V. Vähätalo[†]

[†]Department of Biological and Environmental Science and [‡]Department of Chemistry, University of Jyväskylä, P.O. Box 35, FI-40014 Jyväskylä, Finland

[§]Department of Forest Sciences, University of Helsinki, P.O. Box 27, FI-00014 Helsinki, Finland

[∥]Department of Environmental Sciences, University of Helsinki, P.O. Box 65, FI-00014 Helsinki, Finland

Supporting Information

ABSTRACT: Solar radiation mineralizes dissolved organic matter (DOM) to dissolved inorganic carbon through photochemical reactions (DIC photoproduction) that are influenced by iron (Fe) and pH. This study addressed as to what extent Fe contributes to the optical properties of the chromophoric DOM (CDOM) and DIC photoproduction at different pH values. We created the associations of Fe and DOM (Fe-DOM) that cover the range of loadings of Fe on DOM and pH values found in freshwaters. The introduced Fe enhanced the light absorption by CDOM independent of pH. Simulated solar irradiation decreased the light absorption by CDOM (i.e., caused photobleaching). Fe raised the rate of photobleaching and steepened the spectral slopes of CDOM in low pH but resisted the slope steepening in neutral to alkaline pH. The combination of a low pH (down to pH 4) and high Fe loading on DOM (up to 3.5 μmol mg DOM^{-1}) increased the DIC photoproduction rate and the apparent quantum yields for DIC photoproduction up to 7-fold compared to the corresponding experiments at pH >6 or without Fe. The action spectrum for DIC photoproduction shifted toward the visible spectrum range at low pH in the presence of Fe. Our results demonstrated that Fe can contribute to DIC photoproduction by up to 86% and produce DIC even at the visible spectrum range in acidic waters. However, the stimulatory effect of Fe is negligible at pH >7.

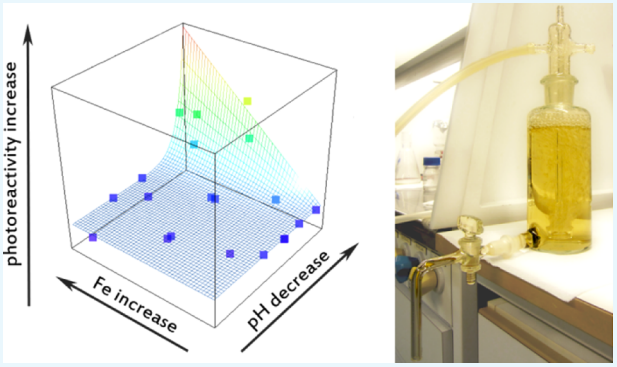

INTRODUCTION

Solar radiation photochemically mineralizes 13−35 Tg C yr^{-1} of dissolved organic carbon (DOC) to dissolved inorganic carbon (DIC) in lakes and reservoirs.[1] Iron (Fe) increases the light absorption by chromophoric dissolved organic matter (CDOM), and therefore influences DIC photoproduction indirectly through changes in the optical properties of CDOM. Solar radiation can mineralize Fe(III)-polycarboxylate complexes of DOM to DIC (Figure S1).[2] Irradiation of Fe can generate reactive oxygen species that mineralize DOC (Figure S1).[3] Low pH enhances Fe-stimulated DIC photoproduction (Figure S1, red circles).[4−6] The recent increases in Fe concentration ([Fe]) and DOC as well as in pH[7−14] emphasize the need to understand the impact of pH and [Fe] on the optical properties of CDOM and DIC photoproduction in freshwaters.

In many surface waters with pH 4−9, ferric iron exists primarily as complexes with DOM and as colloids of iron(oxy)hydroxide stabilized by DOM.[15−19] The colloids stabilized by DOM resist gravitoidal settling, pass filters (e.g., 0.45 μm), and are difficult to separate from Fe complexed by DOM.[15,19,20] In this study, the Fe associated with DOM is abbreviated to Fe-DOM, which includes both the Fe complexes of DOM and the iron(oxy)hydroxide colloids stabilized by DOM.

The importance of Fe stimulus for DIC photoproduction in natural waters has been examined mostly with two approaches: (1) relating DIC photoproduction to water quality parameters and (2) introducing strong complexing ligands for Fe into natural water samples. The first approach has shown that [Fe] and acidity correlate positively with DIC photoproduction.[21−23] According to the second approach, the complexing ligands for Fe reduce DIC photoproduction rates (DICprs).[4,5,23] Both approaches show that [Fe] and acidity play important roles in DIC photoproduction. The quantitative role of Fe on DIC photoproduction remains unclear because the photoreactivity of DOM in natural waters can vary[24] even without Fe and the introduced complexing ligands may potentially interfere with DIC photoproduction.

The DICpr depends on the intensity of irradiation and optical properties of natural waters. Fe(III) enhances light absorption of CDOM, particularly at the longer wavelengths of

Received: April 13, 2017
Accepted: April 21, 2017
Published: May 9, 2017

 © 2017 American Chemical Society

DOI: 10.1021/acsomega.7b00453
ACS Omega 2017, 2, 1905−1914

the visible spectrum range.[25,26] DIC photoproduction and the photoreduction of Fe(III) to Fe(II) increase exponentially with shorter wavelengths of irradiance,[4,27−29] indicating that Fe-stimulated DIC photoproduction has strong spectral dependence. Photon flux densities of solar radiation increase from low values at the UV range to the maximum of the visible spectrum range. The light absorption by CDOM and the photochemical reactivity of DOM are all spectrally dependent due to solar radiation, and spectral dependence should be accounted for the Fe-stimulated DIC photoproduction.

This study quantified the impact of [Fe] and pH on the optical properties of CDOM, the light-induced changes in optical properties, DICprs, and the spectral-apparent quantum yields for DIC photoproduction (ϕ_λ). To generate the associations between Fe(III) and DOM (Fe-DOM), the same concentration (10 mg DOM L^{-1}) of Fe-free DOM isolate from lake water received Fe(III) at different concentrations. Our experiments covered 20 combinations of pH and [Fe], where the pH ranged from 4 to 9.4 and the Fe loadings on DOM were from 0.004 to 3.5 μmol Fe mg DOM^{-1}. Competing multiple regression models were used to find the most parsimonious model that was able to explain the effect of pH and [Fe] on the optical properties of CDOM and DIC photoproduction. On the basis of the modeling, we estimated the magnitude of the Fe-stimulated DIC photoproduction. Determination of ϕ_λ allowed us to evaluate the spectral dependence of DIC photoproduction and showed that Fe shifted the action spectrum of DIC photoproduction towards the visible spectrum range.

RESULTS

Dependence of Optical Properties on pH and [Fe]. When the same DOM concentration (10 mg DOM L^{-1}) was associated with the different Fe concentrations and adjusted to pH values ranging from 4 to 9.4 (Table S2), the absorption coefficient of CDOM at 330 nm (a_{330}) increased with the rising [Fe] (a_{330_Dark} in Figure 1a; "Init." in Table S5). The dependence of a_{330} on [Fe] and pH (expressed as the concentration of hydrogen ion, $[H^+] = 10^{-pH}$ in the models) was analyzed with eight competing regression models (Table S8). The a_{330_Dark} was significantly dependent on [Fe] in all models that included [Fe] as a separate predictor variable (shown as bold regression coefficients $b1$ for the models 2, 4, 6, and 8 in Table S8). In the model 7 without [Fe] as a separate predictor variable, a_{330_Dark} was significantly dependent on pH (term $[H^+]$, coefficient $b2$) and the interaction between pH and [Fe] (term [Fe] $[H^+]$, coefficient $b3$; Table S8). Among the models containing only significant terms (models 1, 2, and 7 in Table S8), the model 2 had the lowest value of AICc (110 in Table S8). Therefore, the model 2 (marked with * in Table S8) was selected to explain the simplest significant dependence of a_{330_Dark} on the predictor variables. According to the best model 2 (Table S8), a_{330_Dark} was significantly dependent on [Fe] alone. The model 2 (Table S8) is illustrated as a surface in Figure 1a together with color-coded dots that show a_{330_Dark} in the 20 experiments (Table S5). In a similar manner, text in the later results section refers to the significant dependencies of the most parsimonious models marked with * in Tables S8−S18, which are also illustrated as surfaces in Figures 1−3.

The Fe associated with DOM increased the absorption coefficient of CDOM at different wavelengths unequally because the spectral slope coefficients ($S_{275-295}$, $S_{350-400}$) decreased with increasing [Fe] associated to DOM (Table S6). The value of $S_{275-295}$ decreased more than that of $S_{350-400}$, which was seen as a decrease in the slope ratio (S_R) (Figure 1b, Table S6). The changes in $S_{275-295}$ (model 2 in Table S9) and S_R (model 2 in Table S10) depended only on [Fe], as illustrated for S_R (Figure 1b). Therefore, the changes in optical properties of CDOM depended only on the introduced [Fe] and not on pH adjustment (Tables S9−S11, Figure 1).

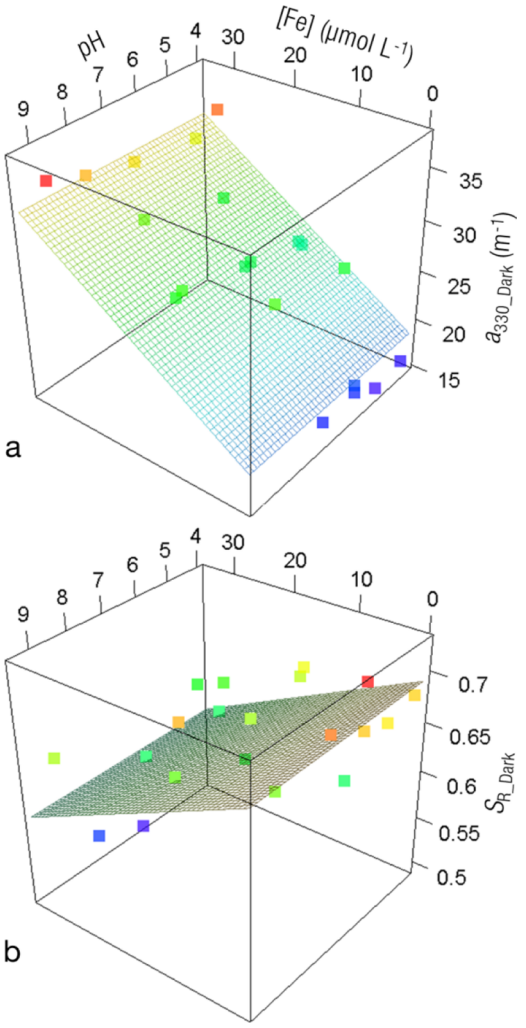

Figure 1. Impact of [Fe] and pH on the optical properties of CDOM represented as (a) the absorption coefficient of CDOM at 330 nm (a_{330_Dark}) and (b) the spectral slope ratio (S_{R_Dark}) in the dark control samples. Dots show the experimental data (Tables S5 and S6), and the surfaces show the fit of the best model on the data (model 2 in both Tables S8 and S10). The color of dots and the surfaces follows the value of the vertical axis. The lowest values are shown in violet, intermediate values with cyan, blue, green, yellow, and orange, and the highest values in red.

Simulated solar irradiation decreased a_{330} (i.e., caused photobleaching) and increased $S_{275-295}$ and S_R values (Tables S5 and S6). The photobleaching of a_{330} (Δa_{330}) and photochemistry-induced change in $S_{275-295}$ ($\Delta S_{275-295}$) and in S_R (ΔS_R) depended positively on the interaction between [Fe] and acidity (Figure 2a,b; model 5 in Table S11, models 6 in Tables S12 and S13). $\Delta S_{275-295}$ and ΔS_R were additionally negatively dependent on [Fe] (Figure 2b; models 6 in Tables S12 and S13).

Rate of DIC Photoproduction at Different pH and [Fe]. Irradiation produced DIC at rates ranging from 1.72 to 12.08

DOI: 10.1021/acsomega.7b00453
ACS Omega 2017, 2, 1905−1914

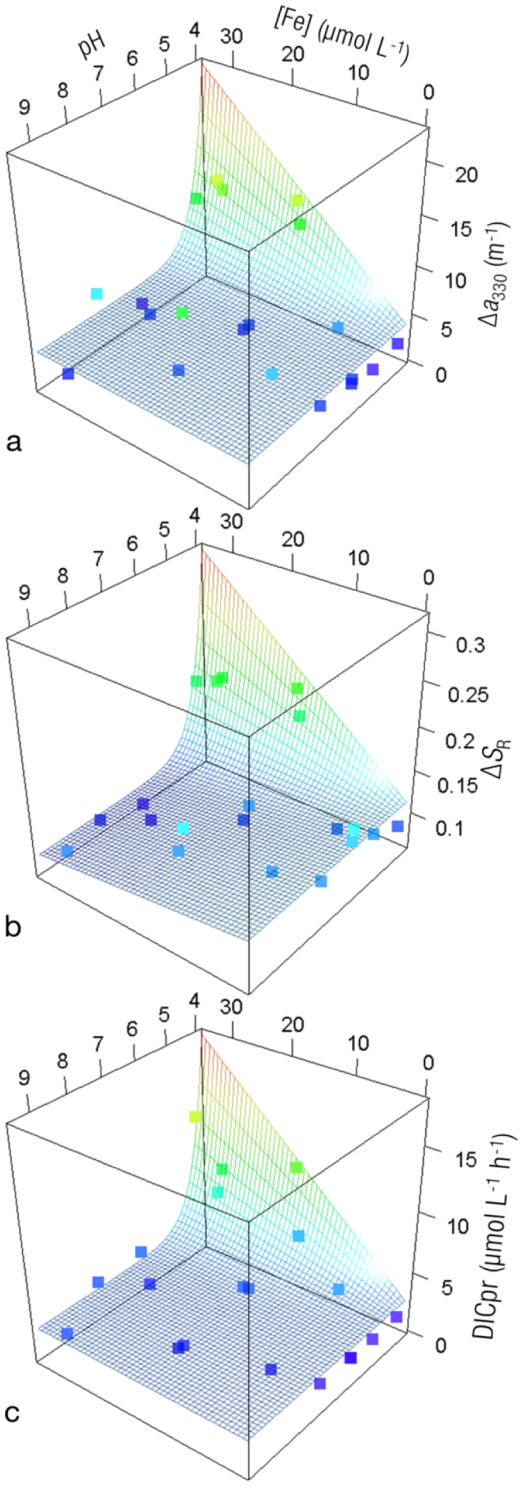

Figure 2. Impact of [Fe] and pH on (a) the photobleaching of a_{330} (Δa_{330}), (b) the photochemistry-induced change in S_R (ΔS_R), and (c) DICpr. Dots show experimental data (Tables S5–S7) and the surfaces show the fit of the best models on data (model 5 in Table S11, model 6 in Table S13 and model 5 in Table S14). Note that the highest values in the surface exceed the experimental data and should be treated with caution. Color-coding is the same as in Figure 1.

μmol C L^{-1} h^{-1} (Table S7). Because each experiment contained an identical concentration (10 mg DOM L^{-1}) of the same solid-phase extracted DOM (SPE-DOM), the up to 7-fold differences in the rate of DIC photoproduction were caused by the experimental adjustments of pH and [Fe]. According to the best model, DICpr was dependent on the interaction between pH and [Fe] (Figure 2c; model 5 in Table S14).

Influence of Fe and pH on ϕ_λ. The calculations of ϕ_λ (details in Supporting Information) accounted for the light absorption by the introduced Fe (Figure 1) and photobleaching of CDOM during the irradiations (Figure 2). The ϕ_λ values are reported in Table S7 with two parameters: c, the apparent quantum yields at wavelength 0 nm ($=\phi_0$) and d, the spectral slope coefficient of ϕ_λ (eq 2). These two parameters allow the calculation of ϕ_λ spectrally, as shown in Figure S5 or at a specific wavelength (e.g., 330 nm; ϕ_{330}, Table S7), which approximates the median wavelength ($\lambda_{50\%}$) that induced DIC photoproduction during the irradiations.

Both ϕ_{330} and c were positively dependent on the interaction between [Fe] and acidity (Figure 3a,b; models 5 in Tables S15 and S16) similar to that found for the rate of DIC photoproduction (Figure 2c; model 5 Table S14). The spectral slope coefficient of ϕ_λ, d, had a similar but negative dependence on the interaction between [Fe] and acidity (Figure 3c, model 5 in Table S17). The rise in c indicated a general increase in ϕ_λ at any wavelength, but the decrease in d meant that ϕ_λ increased relatively more at longer wavelengths.

To demonstrate the role of [Fe] on DIC photoproduction at different pH values, we calculated the relative contribution of Fe-stimulated ϕ_{330} ($\phi_{330,Fe}$) to the total ϕ_{330} ($\phi_{330,total}$) for a few selected [Fe] (Figure 4). When [Fe] was >10 μM, Fe-stimulated reactions dominated DIC photoproduction at pH 4, but their contribution fell to a few percent at pH 6 and was negligible at pH >7 (Figure 4).

Figure 5 compares the largest ϕ_λ at pH 4 with 18 μM [Fe] (experiment #11) to the ϕ_λ without the introduced Fe at a similar pH (#1; Table S7). The Fe-stimulated ϕ_λ is calculated as the difference in ϕ_λs between experiment #11 and #1 (#11−#1, Figure 5, red dotted line). The spectral slope coefficient for ϕ_λ was smaller for the Fe-stimulated DIC photoproduction (d = 0.020 nm^{-1}, Figure 5, red dotted line) than for the corresponding experiment without the introduced Fe (d = 0.025 nm^{-1} in #1, Figure 5, blue dotted line).

To illustrate the potential environmental impact of Fe on DIC photoproduction in acidic waters (pH ≈ 4), we calculated the action spectra for DIC photoproduction per m^2 using a typical daily solar radiation spectrum and the ϕ_λ values reported in Figure 5 (Figure 6). The rate of DIC photoproduction calculated as an integral over 300−700 nm was 2456 μmol C m^{-2} day^{-1} in the presence of 18 μM [Fe] and 5.8 times larger than 424 μmol C m^{-2} day^{-1} in the presence of negligible 0.04 μM [Fe] (Figure 6). Fe shifted the action spectrum toward the visible spectrum range and caused Fe-stimulated DIC photoproduction even at wavelengths >500 nm (Figure 6). At wavelengths >500 nm, Fe stimulus is nearly entirely responsible for DIC photoproduction (Figure 6). The median wavelength for DIC photoproduction ($\lambda_{50\%}$) shifted by 20 nm from 378 (#1) to 398 nm (#11; Figure 6).

DISCUSSION

This study systematically examined the combined impact of pH and introduced Fe(III) onto the optical properties of CDOM, the rates of photoreactions (photobleaching, DIC photoproduction), and the spectral photochemical reactivity (ϕ_λ) of a natural Fe-free isolate of aquatic DOM. Our major findings (summarized in Table 1) imply that Fe can have a strong effect

DOI: 10.1021/acsomega.7b00453
ACS Omega 2017, 2, 1905−1914

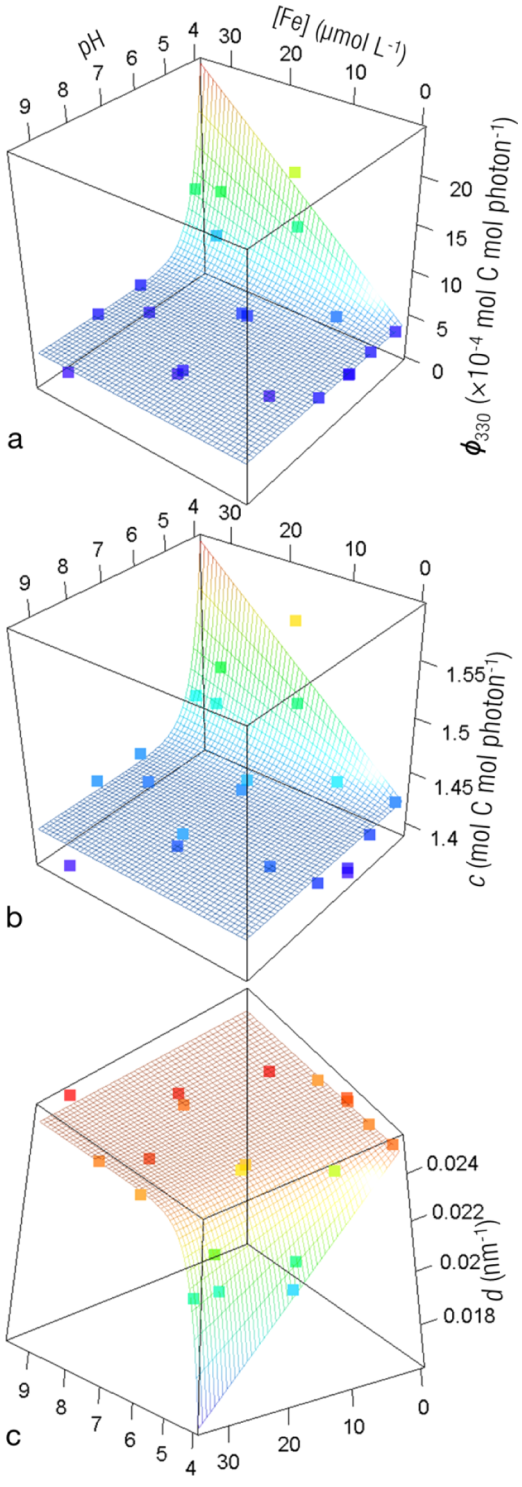

Figure 3. Impact of [Fe] and pH on the apparent quantum yields spectra for DIC photoproduction, ϕ_λ values (a) at 330 nm, ϕ_{330}; (b) c of eq 2; and (c) spectral slope coefficient of ϕ_λ (=d of eq 2). Dots indicate experimental data (Table S7), and the surfaces show the fit of the best model on data (models 5 in Tables S14–S16). Please note that in (c) the orientation of the three-dimensional cube is different.

on the optical properties and photochemistry of DOM, but the effect is often regulated by pH.

Impact of Fe and pH on Optical Properties. As expected for the DOM isolated from a humic lake, its low S_R (≈0.7) is a characteristic of a terrestrial DOM that has entered the aquatic

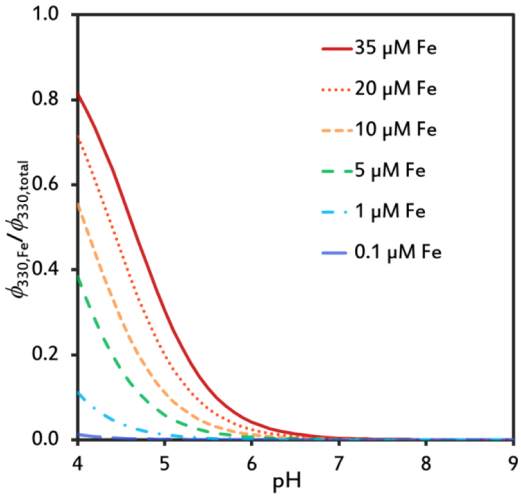

Figure 4. Contribution of Fe to the apparent quantum yields for DIC photoproduction at 330 nm ($\phi_{330,Fe}/\phi_{330,total}$) at the selected [Fe], along a pH gradient. The ratio $\phi_{330,Fe}/\phi_{330,total}$ is calculated from model 5 in Table S15 (also shown as a surface in Figure 3a). According to model 5, $\phi_{330,Fe} = \phi_{330,total} - 3.76 \times 10^{-4}$ (mol C mol photons^{-1}), where the intercept refers to a pH-independent ϕ_{330} without Fe. The concentration of DOM was always 10 mg DOM L^{-1}, therefore, e.g., 35 μM Fe refers to a loading of 3.5 μmol Fe mg DOM^{-1}.

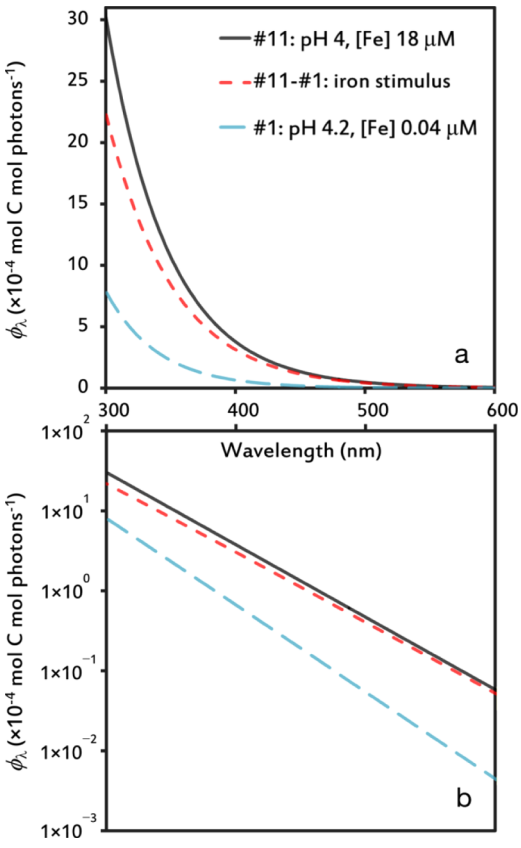

Figure 5. ϕ_λs in acidic (pH ≈ 4) experiments #1 (0.04 μM [Fe]) and #11 (18 μM [Fe]) as well as the Fe-stimulated ϕ_λ calculated as a difference in ϕ_λ values between #11 and #1. c and d are reported in Table S7 for #1 and #11. For the Fe-stimulated ϕ_λ (#11–#1), c = 0.934 mol C mol photons^{-1} and d = 0.0200 nm^{-1}. The same ϕ_λs are shown in (a) linear and (b) in logarithmic scales.

DOI: 10.1021/acsomega.7b00453
ACS Omega 2017, 2, 1905−1914

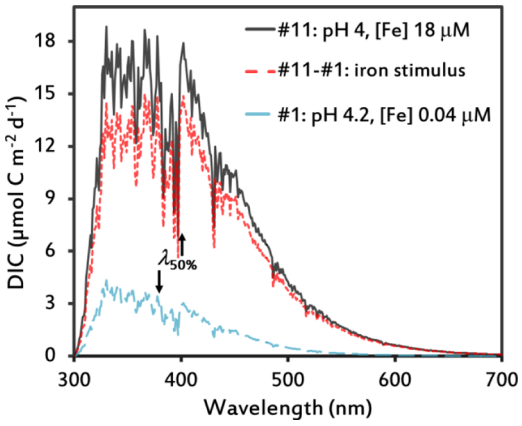

Figure 6. Calculated action spectrum for areal DIC photoproduction at pH 4. DIC photoproduction is calculated as $\int_{\lambda_{300}}^{\lambda_{700}} \phi_\lambda Q_\lambda \, d\lambda$, where ϕ_λ (mol C mol photons^{-1} nm^{-1}) is from experiments #1, #11, or #11−#1 (Figure 5) and Q_λ (mol photons^{-1} m^{-2} day^{-1} nm^{-1}) is the mean daily solar photon flux density at the earth surface averaged across the latitudes (168 W m^{-2} global radiation), having the properties of ASTM G173-03 reference solar spectrum.[41] The arrows show the median wavelength inducing areal DIC photoproduction ($\lambda_{50\%}$), which is 378 nm in #1 without Fe and 398 nm in #11 with 18 μM Fe.

Table 1. Summary of Major Findings in this Study

no.	finding	figure and table
1	Fe stimulates photobleaching of CDOM and increases $S_{275-295}$ and S_R in acidic waters but resists an increase in $S_{275-295}$ and S_R in neutral−alkaline water	Figure 2a,b; Tables S6, S11, and S12
2	DIC photoproduction in Fe-free DOM is pH-independent (pH 4−7)	Figures 2c and S7; Table S7
3	the association of Fe with DOM can enhance the photochemical mineralization rate of DOC 7-fold	Figure 2c
4	Fe contributes 0−86% to DIC photoproduction depending on pH and [Fe]	Figure 4; Table S7
5	the association of Fe with DOM can increase the ϕ_λ for DIC photoproduction by 5-fold	Figure 3a; Table S7
6	the spectral slope coefficient of ϕ_λ for Fe-stimulated DIC photoproduction is low and similar to the corresponding slopes for Fe(III) photoreduction	Figures 5 and S8
7	in acidic water, the association of Fe with DOM shifts the action spectrum of DIC photoproduction toward the visible spectrum range	Figure 6
8	solar radiation >500 nm can potentially mineralize DOC in acidic Fe-rich waters photochemically	Figure 6

regime recently.[38] Our experimental Fe introduction demonstrated that the association of Fe(III) with DOM decreases $S_{275-295}$ more than $S_{350-400}$ when independent of pH and causes a decline in S_R in agreement with earlier studies.[25,26] These observations suggest that Fe(III) associated with DOM contributes to a high a_λ and low S_R that is related to the fresh input of terrestrial CDOM into the aquatic regime.[25,38]

In this study, a_λ increases linearly along the concentration of Fe(III) associated with DOM, consistent with the previous findings.[25,26,42] The rise in a_λ caused by Fe(III) is pH-independent according to this (pH 4−9.4) and an earlier study (pH 2−7).[26] Some studies have reported an increase in a_λ with pH,[42−44] but for waters rich in Fe, this pH effect is smaller than the contribution of Fe(III) to a_λ (this study).[26,42] For instance, 35 μM Fe doubled a_λ and contributed about 50% to the light absorption by Fe(III)-DOM (Table S5). Similar or even higher contributions of Fe to the light absorption by CDOM have been reported in rivers[33] or springs fed by groundwater.[25]

Irradiation decreases (i.e., photobleaches) a_λ and increases S_R according to this and earlier studies.[6,38] In our experiments, these changes in the optical properties of CDOM took place both in the presence and absence of Fe, although to a different degree, depending on the combination of [Fe] and pH. In this study, Fe-stimulated photobleaching increased S_R and $S_{275-295}$ at low pH but resisted these changes in the spectral slopes at high pH (Figure 2a,b; Tables S12 and S13). The stimulatory effect of [Fe] and acidity may be partly related to photoproduced Fe(II), which absorbs light weakly and oxidizes slowly to highly absorbing Fe(III) at low pH.[26,45] Additionally, the same combination (high Fe(III) and low pH) stimulates photoproduction of HO$^\bullet$, which can attack organic chromophores and enhance their photobleaching.[46−48] At high pH, photoproduced Fe(II) is oxidized rapidly back to highly absorbing Fe(III) and the photobleaching of Fe-DOM likely primarily concerns the organic chromophores of CDOM. The chromophores of Fe(III) in nonacidic waters seem to withstand photobleaching similar to iron oxides that are commonly used as weather-resistant outdoor pigments in neutral−alkaline conditions.[49]

Impact of Fe and pH on DIC Photoproduction. According to our irradiation experiments, pH (4−9.4) alone has a nonsignificant impact on DICpr when [Fe] is low (Table S7). Similarly, an earlier study showed that an experimental acidification by one pH unit had a nonsignificant effect on DIC photoproduction in lake waters (pH 4.2−7.2) with low [Fe].[50] Our study showed that Fe stimulates DIC photoproduction in acidic but not in neutral to alkaline conditions. In agreement with our findings, DIC photoproduction was dependent on [Fe] in 38 Swedish lakes, including acidic lakes (pH 4.5−9.5) but the dependence was absent in a subset of 27 lakes having pH >6 (Figure S6).[21] Likewise, in six lakes and two reservoirs (Québec, Canada), the broadband-apparent quantum yields for DIC photoproduction showed a nonsignificant relationship with ambient pH 6.4−8.2.[51] Fe introduction to circumneutral Brandy Lake inflow did not give rise to photochemical loss of DOC.[23] Thus, pH has a minor role on DIC photoproduction in the absence of Fe (ref 50, this study) or in neutral to alkaline waters even in the presence of Fe (refs 21, 23, 51, this study).

Our experiments showed that Fe stimulates DIC photoproduction only in acidic conditions similar to those found earlier in natural water samples.[3−5,21,44,48,50,52] According to our volumetric DICprs (Figure 2c), $\phi_{\lambda s}$ (Figures 3 and 4), or the areal rates calculated from $\phi_{\lambda s}$ (Figure 6), the Fe-stimulated DIC photoproduction is responsible for up to 86% of the total DIC photoproduction at pH ≈ 4 with up to 3.5 μmol Fe mg DOM^{-1}. In the example illustrated in Figure 6 (pH ≈ 4, 1.8 μmol Fe mg DOM^{-1}), Fe contributed 83% to the total DIC photoproduction. The calculated contribution (Figure 5) would fall to 56% at pH 4, with 1 μmol Fe mg DOM^{-1}, which is the highest reported amount of Fe complexed by DOM in natural waters.[18] In typical boreal wetlands and forested streams (pH 4−5; 0.3−0.4 μmol complexed Fe mg DOM^{-1}),[18] the calculated (Figure 5) contribution of Fe to DIC photoproduction is between 4 and 33%. In a strict sense, these calculations apply to our experimental conditions, but they suggest that Fe can contribute up to ≈50% to DIC photoproduction in acidic surface waters.

How Does Iron Stimulate DIC Photoproduction at Low pH? Our study was not designed to address the

DOI: 10.1021/acsomega.7b00453
ACS Omega 2017, 2, 1905−1914

mechanistic details of Fe-stimulated DIC photoproduction, but here, we discuss how our observations fit to the mechanistic understanding gained by earlier studies.[2,3] Fe can contribute to DIC photoproduction through two principal mechanisms: (1) the photochemical decarboxylation of Fe(III)−carboxylate complexes and (2) the photo-Fenton reactions (Figure S1). DOM can bind Fe(III) into Fe(III)−carboxylate complexes ([1], Figure S1). In the first mechanism, a light-induced ligand-to-metal-charge-transfer (LMCT; [2], Figure S1) can decarboxylate the Fe(III)−carboxylate complexes and produce DIC ([3], Figure S1). In the second mechanism, photoproduced ferrous iron (Fe(II)) can reduce dioxygen (O_2) to superoxide/hydroperoxyl radicals ($HO_2^\bullet/O_2^-$; [4], Figure S1). Dismutation of $HO_2^\bullet/O_2^-$ produces hydrogen peroxide (H_2O_2), which can oxidize Fe(II) and generate hydroxyl radicals ($HO^\bullet$) through photo-Fenton reactions ([5] and [9], Figure S1). $HO^\bullet$ can oxidize DOM and produce DIC ([6], Figure S1). A single reaction between DOM and $HO^\bullet$ can release CO_2 ([6], Figure S1), but approximately three moles $HO^\bullet$ are typically needed to produce 1 mol CO_2 from DOM.[53]

Fe-stimulated DIC photoproduction benefits from acidic conditions (refs 23, 50, this study), as indicated with red circles in Figure S1: (i) acidity facilitates complexation of Fe(III) with DOM instead of formation of insoluble Fe(III)(hydr)oxides;[18] (ii) at low pH, O_2^- equilibrates to $HO_2^\bullet$;[54] (iii) acidity promotes the dismutation of $HO_2^\bullet/O_2^-$ to H_2O_2;[54] and (iv) acidity promotes the formation of $HO^\bullet$ instead of a weaker oxidant Fe(IV).[55] Fe-stimulated DIC photoproduction through the photochemical decarboxylation of Fe(III)−carboxylate complexes can be efficient (quantum yields up to 1 in Fe(III)-oxalate),[2] but requires re-formation of Fe(III)−carboxylate complexes that is favored by low pH. Photo-Fenton mechanisms do not necessarily require physical association between DOM and Fe, because numerous species of Fe(III),[56] simple ions ($[Fe(III)\ OH\ (H_2O)_5]^{2+}$),[27] inorganic colloids or solids,[57] or organic complexes[46,58] can efficiently yield Fe(II) and $HO^\bullet$. Our study cannot evaluate the relative importance of the two principal mechanisms for Fe-stimulated DIC production, but both of these mechanisms require photochemical reduction of Fe(III) and benefit from low pH.

ϕ_λs and Spectral Dependence of Fe-Stimulated DIC Photoproduction. The ϕ_{330}s determined in this study have a similar range reported earlier for freshwater, in which the magnitude of the reported ϕ_{330}s depend mostly on the optical properties of DOM but decrease with pH (Figure S7).[1,24,28,37,59,60] The pH dependence of ϕ_{330}s in freshwater (Figure S7) is possibly related to their indigenous Fe because the magnitude of ϕ_{330} depends on the interaction of pH and Fe.

In this study, the spectral slope coefficient of ϕ_λ for Fe-stimulated DIC photoproduction was lower compared to that of the corresponding slope without Fe stimulation (Figure 5). This indicates that the contribution of Fe to DIC photoproduction changes with wavelength. This phenomenon depends in part on the effect of Fe(III) on the optical properties of CDOM (a reduction of spectral slope of CDOM, Table S6)[25,26] but also suggests that Fe is photochemically active at long wavelengths.

All mechanisms for Fe-assisted DIC photoproduction (Figure S1) require the photochemical reduction of Fe(III) to Fe(II). The photoreduction of Fe(III) is involved in the $HO^\bullet$ production from $[Fe(III)\ OH\ (H_2O)_5]^{2+}$[27] and in the photochemical dissolution of lepidocrocite.[29] The apparent quantum yields for these reactions decrease exponentially with wavelength and have spectral slopes similar to those of Fe-stimulated DIC photoproduction (Figure S8). This similarity suggests that the apparent quantum yields for the photochemical reduction of Fe(III) to Fe(II) decreases exponentially with wavelength and determines the spectral dependence of associated reactions (e.g., the photoproduction of $HO^\bullet$,[27] dissolved Fe(II),[29] or DIC (this study)).

Our calculated action spectrum for Fe-stimulated DIC photoproduction at pH 4 was shifted toward the visible spectrum range compared to that for DIC photoproduction without Fe (Figure 6). Although the UV and the short-wavelength visible spectrum range dominate the calculated DIC photoproduction, Fe is almost entirely responsible for DIC photoproduction at the wavelengths >500 nm (Figure 6). Irradiation at 590−630 or 577 nm can photoreduce Fe(III) in lepidocrocite or in Fe(III)-phenolate (quantum yields approximately 10^{-4}), respectively.[29,61] These observations indicate that the light absorption by Fe in the visible spectrum range even at >500 nm can reduce Fe(III)-DOM to Fe(II) and stimulate DIC photoproduction in acidic waters.

Environmental Significance. During the past two to three decades, the export of Fe from land to inland waters has increased and enhanced the role of Fe in water color.[10,12,14,62] Since the 1980s, a reduction in sulfate deposition has raised pH[7,63] and mobilized soil-derived organic matter to aquatic systems.[64,65] This study suggests that these trends may reduce photobleaching of color (or CDOM) and DIC photoproduction in some instances because the chromophores of Fe(III) photobleach poorly and cannot efficiently mediate DIC photoproduction at pH >∼7. In naturally and anthropogenically acidic surfaces or atmospheric waters instead, Fe stimulates the photobleaching of CDOM and can enhance DIC photoproduction remarkably at wavelengths >500 nm.

MATERIALS AND METHODS

Sampling, Extraction of DOM, and Chemicals. Approximately 200 L lake water was collected from the humic Lake Kuivajärvi (0.61 km^2; DOC ≈ 12 mg L^{-1}; total nitrogen ≈ 0.4 mg L^{-1}, total phosphorus ≈ 15 μg L^{-1}; 61°50.743′N, 24°17.134′E; Finland)[30] on October 8, 2013. Water was collected into acid-washed polyethylene containers and filtered through 0.2 μm (Sartobran 300 Sterile Capsule; Sartorius Stedim, Germany) for solid phase extraction (SPE) with Bond Elut PPL cartridges (Agilent Technologies), which previously retained 76% of DOC in humic lake water.[31,32] Prior to SPE, water was acidified to pH ≈ 2 with hydrochloric acid (HCl; Merck, Germany) and equilibrated overnight with 0.01 M fluoride (NaF; Merck, Germany), which was added as a ligand to complex Fe.[4] These complexes and the unbound F^- passed the SPE cartridge during extraction. To evaluate the retention of Fe in the SPE-DOM, we collected water before and after SPE cartridge and preserved the water samples with super-pure nitric acid (Romil, U.K.) for Fe determination. (Total iron measurement is described in the Supporting Information.) The concentration of Fe was 3.42 ± 0.034 and 3.45 ± 0.044 μmol L^{-1} (mean ± SD) in triplicated water samples before and after the SPE cartridge, respectively. The negligible difference indicates that the SPE-DOM was free of Fe within the analytical accuracy (≤0.04 μmol L^{-1}) of determination. In agreement with this finding, the measured concentration of total Fe was 0.04 ± 0.002 μmol L^{-1} in the aqueous solutions of SPE-DOM (10 mg DOM L^{-1}) used for the experiments.

DOI: 10.1021/acsomega.7b00453
ACS Omega 2017, 2, 1905−1914

Ultrapure water (Ultra Clear UV UF TM system; Evoqua Water Technologies) was used in all experiments. The Fe solutions were prepared by dissolving iron (III) sulfate hydrate (AnalaR, VWR International Ltd., U.K.) in 0.1 M HCl. All the quartz- and glassware used in the experiments were soaked in 2% nitric acid (Merck, Germany) for >24 h, rinsed throughout with ultrapure water, and pre-combusted at 450 °C for 4 h.

Experimental Design. To examine the combined impact of pH and concentration of total iron (denoted [Fe]) on the spectral properties of CDOM, the rates of photoreactions (photobleaching, DIC photoproduction), and ϕ_λs, we generated the associations between Fe and DOM (Fe-DOM) using the same concentration of SPE-DOM (10 mg DOM L^{-1}) but different loadings of Fe on DOM at pH values ranging from 4 to 9.4 (Figure S2b, Table S2). The selected Fe loadings on DOM ranged from 0.004 (no introduced Fe) to 3.5 μmol Fe mg DOM^{-1} (the highest amount of introduced Fe; Table S2, Figure S2b). The lowest loading represented the small amount of Fe that was associated to SPE-DOM despite our attempts to isolate entirely Fe-free DOM using a Fe-complexing ligand (F^-) during the extraction. Our lowest loading was substantially smaller than the median (0.357 μmol Fe mg DOM^{-1}) found in large Swedish and Canadian lakes among 58 888 water samples examined.[1] The largest loading was representative of the upper 10% of loadings (2.0−12.8 μmol Fe mg DOM^{-1}) observed in 6128 Finnish river water samples.[33] Our lowest experimental pH (pH 4) corresponded to that found in naturally acidic boreal streams[18] or acidified atmospheric waters.[34] The highest experimental pH (pH 9.4) represented pH values found in alkaline soda lakes or even in circumneutral lakes during algal blooms.[35]

To find the optimal combinations of [Fe] and pH values across the anticipated range of loadings and pH, we selected nine combinations according to a central-composite design and replicated five of them (Figure S2, Tables S1 and S2). To highlight the effect of pH with high [Fe] and without Fe, we introduced five additional combinations from pH 4 to 9.4 and from 0.004 to 3.5 μmol Fe mg DOM^{-1}, which resulted in a total of 20 experiments (Table S2, Figure S2). The Pearson correlation coefficient between [Fe] and pH was 0.09 (p value >0.1), showing that the selected combinations of pH and [Fe] were not correlated and that pH and [Fe] were independent predictor variables in the statistical analyses.

To evaluate the changes in optical properties and to measure DIC photoproduction, the selected 20 combinations of Fe-DOM were exposed to simulated solar radiation. The optical properties were measured prior to irradiation, from the irradiated Fe-DOM and their corresponding dark controls. For the determination of ϕ_λs, the DIC photoproduction was related to the number of absorbed photons by CDOM.

Preparation of Fe-DOM. The acidic (pH ≈ 1.2) solutions for experiments were prepared as a 1:1 mixture of SPE-DOM solution and Fe(III) solution in a 500 mL gas exchange flask (see the graphical abstract) to final concentrations of 10 mg DOM L^{-1} and [Fe] between 0 and 35 μmol of the introduced Fe(III) L^{-1} (Table S2). The solutions were adjusted to pH 2 with NaOH and bubbled with CO_2-free air (2 L min^{-1}) for 30−45 min to reduce the background DIC concentration. To associate Fe(III) with DOM, the pH of solutions inside the gas exchange flasks were raised slowly with NaOH to the selected pH values (Table S2, Figure S2b). This type of titration leads to the mononuclear binding of Fe on DOM[36] or to the colloids of Fe(III)(oxy)hydroxide stabilized by DOM.[19,20] According to a chemical equilibrium modeling described in the Supporting Information, Fe(III) was bound entirely on DOM in the experiments #1−13 at ≤1.8 μmol Fe mg DOM^{-1} but in the experiments #14−20 up to 28% of Fe(III) existed as iron(oxy)hydroxides (Table S2). No visual precipitates were observed at any stage of the experiments. The absence of precipitates suggested that Fe(III)(oxy)hydroxide colloids were stabilized by DOM.[19,20] For the statistical analyses, we used the total concentration of Fe in the experiments because both Fe complexed by DOM and iron(oxy)hydrodixes affect optical properties[25,26] and can induce DIC photoproduction.[2,3]

Each Fe-DOM solution was tapped in a set of one quartz and two glass vials overflowing with a volume of the vial (∼12 mL) more than three times and sealed without headspace using ground glass stoppers. The quartz vial was exposed to simulated solar radiation (labeled "irradiated"). One glass vial was placed in an ice water bath (0 °C; "initial"). The other glass vial was wrapped in aluminum foil ("dark control") but otherwise treated identically as the quartz vial.

Simulated Solar Irradiation. Solutions in quartz vials were irradiated for 5 h (765 W m^{-2}) using an Atlas Suntest CPS+ solar simulator (Atlas Material Testing Technology), as described previously[37] and in the Supporting Information. For the irradiation at +20 °C, the quartz vials were placed on a stainless steel grid immersed in a water bath, along with the dark controls. The spectral photon flux densities (mol photons m^{-2} s^{-1} nm^{-1}) incident to the quartz vials from above and below were measured from 240 to 800 nm at 1 nm intervals with a spectroradiometer (SR991; Macam Photometrics, Scotland, U.K.). These measurements, together with characterization of downwelling and upwelling light fields, allowed us to calculate the spectral absorption of photons by CDOM in the irradiated samples, accounting for vial dimension, inner filtering effects, and CDOM photobleaching during irradiation (Supporting Information).

Analytical Measurements. After the irradiation, the DIC concentration and the spectral absorption by CDOM was measured from the irradiated, dark control, and initial samples. The DIC concentration was determined as a median of multiple (n = 3) injections into an inorganic carbon reaction vessel of a TOC analyzer (TOC-L_{CPH}; Shimadzu, Japan; detection limit 0.3 μmol C L^{-1}). The analyzer was 6-point calibrated with sodium hydrogen carbonate (Nacalai Tesque Inc., Japan) standard solutions on each measurement day. The analytical precision ranged from 0.18 to 2 μmol C L^{-1} for individual DIC determination, with a median of 0.28 μmol C L^{-1} for all determinations. The concentration of DIC was identical in the initial and dark control samples (95% confidence intervals for the difference were between −0.51 and 0.18 μmol C L^{-1}). This lack of difference indicated that all vials received initially the same DIC concentration and that any dark processes modifying the DIC concentration were negligible. DIC photoproduction was calculated as the difference in the DIC concentration between the irradiated and the corresponding dark control sample.

The spectral absorption by CDOM was measured with a UV−vis spectrophotometer (Lambda 850; PerkinElmer) in a 1 cm quartz cuvette. The apparent absorbance of CDOM and blanks (ultrapure water) was first measured from 190 to 700 nm at 1 nm steps against air (i.e., an empty reference cell holder). The absorption coefficient of CDOM at wavelength λ (a_λ; m^{-1}) was calculated from eq 1

DOI: 10.1021/acsomega.7b00453
ACS Omega 2017, 2, 1905−1914

$$a_\lambda = 2.303(A_{\text{solution},\lambda} - A_{\text{blank},\lambda})l^{-1} \quad (1)$$

where $A_{\text{solution},\lambda}$ and $A_{\text{blank},\lambda}$ are the apparent absorbance of DOM solution and blank, respectively, and l is the path length of the cuvette (m).

The CDOM spectral slope coefficients were calculated as a linear fit to ln-transformed a_λ for two spectral regions: 275−295 nm ($S_{275-295}$; nm^{-1}) and 350−400 nm ($S_{350-400}$; nm^{-1}). The slope ratio (S_R; dimensionless) was expressed as $S_R = S_{275-295}(S_{350-400})^{-1}$, according to Helms et al.[38]

The initial and its corresponding dark control samples had identical a_λ, $S_{275-295}$, $S_{350-400}$, and S_R (Tables S5, S6), indicating negligible changes in the optical properties of CDOM due to the sample treatment without the irradiation. The photochemistry-induced changes in optical properties were calculated by subtracting the values of dark controls from those of irradiated solutions.

Calculation of AQY Spectrum. The ϕ_λ (mol C mol photons^{-1} at wavelength λ) was calculated by dividing the amount of photoproduced DIC with the number of photons absorbed by CDOM in the Fe-DOM solutions during the irradiations as in Aarnos et al.[37] but now with a Monte Carlo approach (details in Supporting Information). In these calculations, it was assumed that ϕ_λ decreases exponentially with increasing wavelength.

$$\phi_\lambda = c\, e^{-d\lambda} \quad (2)$$

where c represents AQY (mol C mol photons^{-1}) at the reference wavelength (0 nm) and d is spectral slope coefficient for ϕ_λ (nm^{-1}). This assumption was adapted from the earlier determinations of ϕ_λ for DIC photoproduction (Supporting Information) and for Fe(III) photoreduction.[27,29]

Statistical Analyses. The dependencies of the optical properties of CDOM and the photochemical transformations of DOM on [Fe] and pH were explored with eight competing regression models (Supporting Information, Tables S8−S18). The models tested the explanatory power of [Fe] and pH separately, together, or through the interaction of [Fe] and pH (Tables S8−S18). For the statistical analyses, pH was expressed as the concentration of hydrogen ion ($[H^+]$; $= 10^{-pH}$) using the same unit (mol L^{-1}) as for [Fe]. For the visualization of models in Figures 1−4, $[H^+]$ was transformed back to pH. To identify the simplest statistically significant dependence between the response and the predictor variables, we sought for the most parsimonious model among those candidate models that included only significant terms. From those models, the best one was selected on the basis of the corrected Akaike Information Criterion (AICc)[39,40] to provide the simplest significant dependence of the optical properties or photochemical transformation of DOM on pH and [Fe]. Statistical analyses were performed using MATLAB R2013a (The MathWorks Inc.) and R (version 3.3.3, R Core Team 2017).

■ ASSOCIATED CONTENT

Supporting Information

The Supporting Information is available free of charge on the ACS Publications website at DOI: 10.1021/acsomega.7b00453.

Scheme for the major reactions involved in the Fe-stimulated DIC photoproduction; the method for the determination of Fe; details of the experimental design; the speciation of Fe(III) in the experiments; details of the method for the determination of ϕ_λ and the uncertainty estimates for ϕ_λs; the data for the optical properties, the DICprs and ϕ_λs from the individual experiments; the regression analyses with the competing models; three figures supporting the discussion; and accompanying references (PDF)

■ AUTHOR INFORMATION

Corresponding Author

*E-mail: yufei.y.gu@jyu.fi. Tel: +358 40 480 2691.

ORCID

Yufei Gu: 0000-0002-6606-2592

Notes

The authors declare no competing financial interest.

■ ACKNOWLEDGMENTS

This study was funded by the University of Jyväskylä and Academy of Finland Centre of Excellence (grant 272041). We thank Jaana Bäck for financial support, Derek K. Ho for linguistic corrections, Veli-Mikko S. Puupponen for technique support concerning AQY fitting, Ari Väisänen for advice on iron determination, and Yihua Xiao for help in sampling and preparation.

■ REFERENCES

(1) Koehler, B.; Landelius, T.; Weyhenmeyer, G. A.; Machida, N.; Tranvik, L. J. Sunlight-induced carbon dioxide emissions from inland waters. *Global Biogeochem. Cycles* **2014**, *28*, 696−711.

(2) Faust, B. C.; Zepp, R. G. Photochemistry of aqueous iron(III)-polycarboxylate complexes: roles in the chemistry of atmospheric and surface waters. *Environ. Sci. Technol.* **1993**, *27*, 2517−2522.

(3) Voelker, B. M.; Morel, F. M. M.; Sulzberger, B. Iron redox cycling in surface waters: effects of humic substances and light. *Environ. Sci. Technol.* **1997**, *31*, 1004−1011.

(4) Gao, H.; Zepp, R. G. Factors influencing photoreactions of dissolved organic matter in a coastal river of the southeastern United States. *Environ. Sci. Technol.* **1998**, *32*, 2940−2946.

(5) Wu, F. C.; Mills, R. B.; Cai, Y. R.; Evans, R. D.; Dillon, P. J. Photodegradation-induced changes in dissolved organic matter in acidic waters. *Can. J. Fish. Aquat. Sci.* **2005**, *62*, 1019−1027.

(6) Helms, J. R.; Mao, J.; Schmidt-Rohr, K.; Abdulla, H.; Mopper, K. Photochemical flocculation of terrestrial dissolved organic matter and iron. *Geochim. Cosmochim. Acta* **2013**, *121*, 398−413.

(7) Vuorenmaa, J.; Forsius, M.; Mannio, J. Increasing trends of total organic carbon concentrations in small forest lakes in Finland from 1987 to 2003. *Sci. Total Environ.* **2006**, *365*, 47−65.

(8) Monteith, D. T.; Stoddard, J. L.; Evans, C. D.; de Wit, H. A.; Forsius, M.; Hogasen, T.; Wilander, A.; Skjelkvale, B. L.; Jeffries, D. S.; Vuorenmaa, J.; Keller, B.; Kopacek, J.; Vesely, J. Dissolved organic carbon trends resulting from changes in atmospheric deposition chemistry. *Nature* **2007**, *450*, 537−540.

(9) Keller, W.; Paterson, A. M.; Somers, K. M.; Dillon, P. J.; Heneberry, J.; Ford, A. Relationships between dissolved organic carbon concentrations, weather, and acidification in small Boreal Shield lakes. *Can. J. Fish. Aquat. Sci.* **2008**, *65*, 786−795.

(10) Neal, C.; Lofts, S.; Evans, C. D.; Reynolds, B.; Tipping, E.; Neal, M. Increasing iron concentrations in UK upland waters. *Aquat. Geochem.* **2008**, *14*, 263−288.

(11) Haaland, S.; Hongve, D.; Laudon, H.; Riise, G.; Vogt, R. D. Quantifying the drivers of the increasing colored organic matter in boreal surface waters. *Environ. Sci. Technol.* **2010**, *44*, 2975−2980.

(12) Kritzberg, E. S.; Ekström, S. M. Increasing iron concentrations in surface waters − a factor behind brownification? *Biogeosciences* **2012**, *9*, 1465−1478.

(13) Oni, S. K.; Futter, M. N.; Bishop, K.; Köhler, S. J.; Ottosson-Löfvenius, M.; Laudon, H. Long-term patterns in dissolved organic

DOI: 10.1021/acsomega.7b00453
ACS Omega 2017, 2, 1905−1914

carbon, major elements and trace metals in boreal headwater catchments: trends, mechanisms and heterogeneity. *Biogeosciences* **2013**, *10*, 2315−2330.
(14) Kritzberg, E. S.; Villanueva, A. B.; Jung, M.; Reader, H. E. Importance of boreal rivers in providing iron to marine waters. *PLoS One* **2014**, *9*, No. e107500.
(15) Gustafsson, C.; Gschwend, P. M. Aquatic colloids: Concepts, definitions, and current challenges. *Limnol. Oceanogr.* **1997**, *42*, 519−528.
(16) Gustafsson, Ö.; Widerlund, A.; Andersson, P. S.; Ingri, J.; Roos, P.; Ledin, A. Colloid dynamics and transport of major elements through a boreal river — brackish bay mixing zone. *Mar. Chem.* **2000**, *71*, 1−21.
(17) Ingri, J.; Widerlund, A.; Land, M.; Gustafsson, Ö.; Andersson, P.; Öhlander, B. Temporal variations in the fractionation of the rare earth elements in a boreal river; the role of colloidal particles. *Chem. Geol.* **2000**, *166*, 23−45.
(18) Neubauer, E.; Köhler, S. J.; von der Kammer, F.; Laudon, H.; Hofmann, T. Effect of pH and stream order on iron and arsenic speciation in boreal catchments. *Environ. Sci. Technol.* **2013**, *47*, 7120−7128.
(19) Chen, K.-Y.; Chen, T.-Y.; Chan, Y.-T.; Cheng, C.-Y.; Tzou, Y.-M.; Liu, Y.-T.; Teah, H.-Y. Stabilization of natural organic matter by short-range-order iron hydroxides. *Environ. Sci. Technol.* **2016**, *50*, 12612−12620.
(20) Philippe, A.; Schaumann, G. E. Interactions of dissolved organic matter with natural and engineered inorganic colloids: a review. *Environ. Sci. Technol.* **2014**, *48*, 8946−8962.
(21) Bertilsson, S.; Tranvik, L. J. Photochemical transformation of dissolved organic matter in lakes. *Limnol. Oceanogr.* **2000**, *45*, 753−762.
(22) Anesio, A. M.; Granéli, W. Increased photoreactivity of DOC by acidification: Implications for the carbon cycle in humic lakes. *Limnol. Oceanogr.* **2003**, *48*, 735−744.
(23) Porcal, P.; Dillon, P. J.; Molot, L. A. Interaction of extrinsic chemical factors affecting photodegradation of dissolved organic matter in aquatic ecosystems. *Photochem. Photobiol. Sci.* **2014**, *13*, 799−812.
(24) Koehler, B.; Broman, E.; Tranvik, L. J. Apparent quantum yield of photochemical dissolved organic carbon mineralization in lakes. *Limnol. Oceanogr.* **2016**, *61*, 2207−2221.
(25) Xiao, Y.; Sara-Aho, T.; Hartikainen, H.; Vähätalo, A. V. Contribution of ferric iron to light absorption by chromophoric dissolved organic matter. *Limnol. Oceanogr.* **2013**, *58*, 653−662.
(26) Poulin, B. A.; Ryan, J. N.; Aiken, G. R. Effects of iron on optical properties of dissolved organic matter. *Environ. Sci. Technol.* **2014**, *48*, 10098−10106.
(27) Benkelberg, H.; Warneck, P. Photodecomposition of iron (III) hydroxo and sulfato complexes in aqueous solution: wavelength dependence of OH and SO_4^- quantum yields. *J. Phys. Chem.* **1995**, *99*, 5214−5221.
(28) Vähätalo, A. V.; Salkinoja-Salonen, M.; Taalas, P.; Salonen, K. Spectrum of the quantum yield for photochemical mineralization of dissolved organic carbon in a humic lake. *Limnol. Oceanogr.* **2000**, *45*, 664−676.
(29) Borer, P.; Sulzberger, B.; Hug, S. J.; Kraemer, S. M.; Kretzschmar, R. Wavelength-dependence of photoreductive dissolution of lepidocrocite (γ-FeOOH) in the absence and presence of the siderophore DFOB. *Environ. Sci. Technol.* **2009**, *43*, 1871−1876.
(30) Miettinen, H.; Pumpanen, J.; Heiskanen, J. J.; Aaltonen, H.; Mammarella, I.; Ojala, A.; Levula, J.; Rantakari, M. M. Towards a more comprehensive understanding of lacustrine greenhouse gas dynamics - two -year measurements of concentrations and fluxes of CO_2, CH_4 and N_2O in a typical boreal lake surrounded by managed forests. *Boreal Environ. Res.* **2015**, *20*, 75−89.
(31) Dittmar, T.; Koch, B.; Hertkorn, N.; Kattner, G. A simple and efficient method for the solid-phase extraction of dissolved organic matter (SPE-DOM) from seawater. *Limnol. Oceanogr.: Methods* **2008**, *6*, 230−235.
(32) Xiao, Y.; Hoikkala, L.; Kasurinen, V.; Tiirola, M.; Kortelainen, P.; Vähätalo, A. V. The effect of iron on the biodegradation of natural dissolved organic matter. *J. Geophys. Res.: Biogeosci.* **2016**, *121*, 2544−2561.
(33) Xiao, Y.-H.; Räike, A.; Hartikainen, H.; Vähätalo, A. V. Iron as a source of color in river waters. *Sci. Total Environ.* **2015**, *536*, 914−923.
(34) Amato, P.; Ménager, M.; Sancelme, M.; Laj, P.; Mailhot, G.; Delort, A. Microbial population in cloud water at the Puy de Dôme: Implications for the chemistry of clouds. *Atmos. Environ.* **2005**, *39*, 4143−4153.
(35) López-Archilla, A. I.; Moreira, D.; López-García, P.; Guerrero, C. Phytoplankton diversity and cyanobacterial dominance in a hypereutrophic shallow lake with biologically produced alkaline pH. *Extremophiles* **2004**, *8*, 109−115.
(36) Karlsson, T.; Persson, P. Complexes with aquatic organic matter suppress hydrolysis and precipitation of Fe(III). *Chem. Geol.* **2012**, *322*−*323*, 19−27.
(37) Aarnos, H.; Ylöstalo, P.; Vähätalo, A. V. Seasonal photo-transformation of dissolved organic matter to ammonium, dissolved inorganic carbon, and labile substrates supporting bacterial biomass across the Baltic Sea. *J. Geophys. Res.: Biogeosci.* **2012**, *117* 10.1029/2010JG001633.
(38) Helms, J. R.; Stubbins, A.; Ritchie, J. D.; Minor, E. C.; Kieber, D. J.; Mopper, K. Absorption spectral slopes and slope ratios as indicators of molecular weight, source, and photobleaching of chromophoric dissolved organic matter. *Limnol. Oceanogr.* **2008**, *53*, 955−969.
(39) Anderson, D. R.; Burnham, K. P.; White, G. C. AIC model selection in overdispersed capture-recapture data. *Ecology* **1994**, *75*, 1780−1793.
(40) Burnham, K. P.; Anderson, D. R. Multimodel inference: understanding AIC and BIC in model selection. *Sociol. Methods Res.* **2004**, *33*, 261−304.
(41) Kiehl, J. T.; Trenberth, K. E. Earth's annual global mean energy budget. *Bull. Am. Meteorol. Soc.* **1997**, *78*, 197−208.
(42) Weishaar, J. L.; Aiken, G. R.; Bergamaschi, B. A.; Fram, M. S.; Fujii, R.; Mopper, K. Evaluation of specific ultraviolet absorbance as an indicator of the chemical composition and reactivity of dissolved organic carbon. *Environ. Sci. Technol.* **2003**, *37*, 4702−4708.
(43) Baes, A. U.; Bloom, P. R. Fulvic acid ultraviolet-visible spectra: influence of solvent and pH. *Soil Sci. Soc. Am. J.* **1990**, *54*, 1248−1254.
(44) Porcal, P.; Dillon, P. J.; Molot, L. A. Seasonal changes in photochemical properties of dissolved organic matter in small boreal streams. *Biogeosciences* **2013**, *10*, 5533−5543.
(45) Collienne, R. H. Photoreduction of iron in the epilimnion of acidic lakes. *Limnol. Oceanogr.* **1983**, *28*, 83−100.
(46) Southworth, B. A.; Voelker, B. M. Hydroxyl radical production via the photo-Fenton reaction in the presence of fulvic acid. *Environ. Sci. Technol.* **2003**, *37*, 1130−1136.
(47) White, E. M.; Vaughan, P. P.; Zepp, R. G. Role of the photo-Fenton reaction in the production of hydroxyl radicals and photobleaching of colored dissolved organic matter in a coastal river of the southeastern United States. *Aquat. Sci.* **2003**, *65*, 402−414.
(48) Molot, L.; Hudson, J.; Dillon, P.; Miller, S. Effect of pH on photo-oxidation of dissolved organic carbon by hydroxyl radicals in a coloured, softwater stream. *Aquat. Sci.* **2005**, *67*, 189−195.
(49) Cornell, R. M.; Schwertmann, U. *The Iron Oxides: Structure, Properties, Reactions, Occurrences and Uses*; John Wiley & Sons, 2003.
(50) Anesio, A. M.; Granéli, W. Photochemical mineralization of dissolved organic carbon in lakes of differing pH and humic content. *Arch. Hydrobiol.* **2004**, *160*, 105−116.
(51) Soumis, N.; Lucotte, M.; Larose, C.; Veillette, F.; Canuel, R. Photomineralization in a boreal hydroelectric reservoir: a comparison with natural aquatic ecosystems. *Biogeochemistry* **2007**, *86*, 123−135.
(52) Miles, C. J.; Brezonik, P. L. Oxygen consumption in humic-colored waters by a photochemical ferrous-ferric catalytic cycle. *Environ. Sci. Technol.* **1981**, *15*, 1089−1095.
(53) Goldstone, J. V.; Pullin, M. J.; Bertilsson, S.; Voelker, B. M. Reactions of hydroxyl radical with humic substances: bleaching,

DOI: 10.1021/acsomega.7b00453
ACS Omega 2017, 2, 1905−1914

mineralization, and production of bioavailable carbon substrates. *Environ. Sci. Technol.* **2002**, *36*, 364−372.
(54) Bielski, B. H. J.; Cabelli, D. E.; Arudi, R. L.; Ross, A. B. Reactivity of HO_2/O^-_2 radicals in aqueous solution. *J Phys. Chem. Ref. Data* **1985**, *14*, 1041−1100.
(55) Hug, S. J.; Leupin, O. Iron-catalyzed oxidation of arsenic(III) by oxygen and by hydrogen peroxide: pH-dependent formation of oxidants in the Fenton reaction. *Environ. Sci. Technol.* **2003**, *37*, 2734−2742.
(56) Mcknight, D. M.; Kimball, B. A.; Bencala, K. E. Iron photoreduction and oxidation in an acidic mountain stream. *Science* **1988**, *240*, 637−640.
(57) Vermilyea, A. W.; Voelker, B. M. Photo-Fenton reaction at near neutral pH. *Environ. Sci. Technol.* **2009**, *43*, 6927−6933.
(58) Zepp, R. G.; Faust, B. C.; Hoigne, J. Hydroxyl radical formation in aqueous reactions (pH 3−8) of iron(II) with hydrogen peroxide: the photo-Fenton reaction. *Environ. Sci. Technol.* **1992**, *26*, 313−319.
(59) Vähätalo, A. V.; Wetzel, R. G. Photochemical and microbial decomposition of chromophoric dissolved organic matter during long (months−years) exposures. *Mar. Chem.* **2004**, *89*, 313−326.
(60) Groeneveld, M.; Tranvik, L.; Natchimuthu, S.; Koehler, B. Photochemical mineralisation in a boreal brown water lake: considerable temporal variability and minor contribution to carbon dioxide production. *Biogeosciences* **2016**, *13*, 3931−3943.
(61) Kunkely, H.; Vogler, A. Photoredox reactivity of iron (III) phenolates in aqueous solution induced by ligand-to-metal charge transfer excitation. *Inorg. Chem. Commun.* **2003**, *6*, 1335−1337.
(62) Knorr, K.-H. DOC-dynamics in a small headwater catchment as driven by redox fluctuations and hydrological flow paths – are DOC exports mediated by iron reduction/oxidation cycles? *Biogeosciences* **2013**, *10*, 891−904.
(63) Battarbee, R. W.; Shilland, E. M.; Kernan, M.; Monteith, D. T.; Curtis, C. J. Recovery of acidified surface waters from acidification in the United Kingdom after twenty years of chemical and biological monitoring (1988−2008). *Ecol. Indic.* **2014**, *37*, 267−273.
(64) Evans, C. D.; Monteith, D. T.; Cooper, D. M. Long-term increases in surface water dissolved organic carbon: Observations, possible causes and environmental impacts. *Environ. Pollut.* **2005**, *137*, 55−71.
(65) Ekström, S. M.; Sandahl, M.; Nilsson, P. A.; Kleja, D. B.; Kritzberg, E. S. Reactivity of dissolved organic matter in response to acid deposition. *Aquat. Sci.* **2016**, *78*, 463−475.

DOI: 10.1021/acsomega.7b00453
ACS Omega 2017, 2, 1905−1914